Available online at www.sciencedirect.com

SciVerse ScienceDirect

Ceramics International 39 (2013) 6145–6152

CERAMICS INTERNATIONAL

www.elsevier.com/locate/ceramint

The interaction of plasma proteins with nano-size fluoride-substituted apatite powders

L. Montazeri[a,b], J. Javadpour[a,*], M.A. Shokrgozar[b], S. Bonakdar[b,**], M. Khayyat Moghaddam[b], V. Asgary[b]

[a]*School of Metallurgy and Materials Engineering, Iran University of Science and Technology, Tehran, Iran*
[b]*National Cell Bank of Iran, Pasteur Institute of Iran, Tehran, Iran*

Received 13 October 2012; received in revised form 10 January 2013; accepted 12 January 2013
Available online 21 January 2013

Abstract

Phase pure (HAp) and fluoride-substituted apatite (FHAp) powders were synthesized by the hydrothermal method and their specific surface area was determined by atomic force microscopy (AFM). Human osteoblast cells were used to evaluate the bioactivity of the samples. The influence of fluoride ions on the alteration of cell medium components was analyzed using UV–visible spectroscopy in different exposure times. The protein interaction behavior with the pure and substituted powders was assessed by the Bradford method and SDS-PAGE analysis. The mRNA expression level was detected by real time PCR and it was observed that the presence of an optimal level of fluoride ions in the apatite structure has an inductive effect on collagen I and alkaline phosphatase (ALP) expression levels. A similar trend was also observed in the protein adsorption profile indicating that the fluoride content in the apatite lattice has a significant impact on controlling its biological performance. The maximum protein adsorption was observed on the sample with the chemical composition of $Ca_{10}(PO4)_6(OH)_{1.33}F_{0.67}$.

Keywords: Fluoro-hydroxyapatite; Protein adsorption; Bioactivity; Osteoblast

1. Introduction

The extensive use of stoichiometric synthetic hydroxyapatite (HAp) in the biomedical field is based on its chemical similarity to the inorganic components of bones and teeth [1]. However, in the biological environment substituted (cation and/or anion) hydroxyapatite may be formed as a result of exposure to the dissimilar enriched media [2]. For example, administration of therapeutic drugs such as sodium fluoride results in the release of fluoride ions in the physiological environment leading to the formation of fluoride-substituted hydroxyapatite [3]. Besides, different ions including silicon, fluorine or magnesium can be substituted in the structure of hydroxyapatite during synthesis process [4–6]. Such substitutions can modify solubility, bone forming capability and mechanical properties of hydroxyapatite biomaterials [7]. For instance, the positive influence of fluoride ion substitution on the proliferation and differentiation of osteoblast cells has already been reported in the literature [8–10]. In addition, due to its high resistance to biodegradation fluoride-substituted hydroxyapatite has also been used as surface coatings on various orthopedic and dental implants [11]. Even though, there is a general agreement on the favorable effects of fluoride ions in stimulating osteoblastic responses, further study is still required to better understand the nature of the interaction between biomaterials and bone-forming cells and also blood proteins in general [12–14]. In a previous work conducted by the present authors [15], the osteoblast response to the fluoride-substituted apatite powders synthesized by the hydrothermal method was evaluated. The highest proliferation rate as well as ALP

*Correspondence to: Iran University of Science and Technology, Narmak, Postal Code 1684613114, Tehran, Iran. Tel.: +98 21 77240540 50.
**Correspondence to: Pasteur Institute of Iran (IPI), No. 358, 12th Farwardin Ave, Jomhhoori St, Postal Code 1316943551, Tehran, Iran. Tel.: +98 21 66953311 20; fax: +98 21 66465132.
E-mail addresses: javadpourj@iust.ac.ir (J. Javadpour), sh_bonakdar@pasteur.ac.ir (S. Bonakdar).

0272-8842/$ - see front matter © 2013 Elsevier Ltd and Techna Group S.r.l. All rights reserved.
http://dx.doi.org/10.1016/j.ceramint.2013.01.033

activity was observed in the sample containing an optimum level of fluoride ions. The main objective in the present study was to assess and provide a more quantitative evaluation of the osteoblast activity with the variation of fluoride ion content in the hydroxyapatite structure. In particular, the effect of this variation on plasma protein adsorption and osteoblast gene expression was investigated.

2. Materials and methods

2.1. Powder synthesis

Analytical grade calcium hydroxide ($Ca(OH)_2$, Merck, Germany), di-ammonium hydrogen phosphate ($(NH_4)_2HPO_4$, Merck, Germany) and sodium fluoride (NaF, Labachemie, India) were used as raw materials for the synthesis of pure and fluoride-substituted apatite samples. Fetal bovine serum (FBS, Seromed, Germany) and Roswell Park Memorial Institute (RPMI, GIBCO, Scotland) were used in biological assays. The details of the powder synthesis method were described in our previous work [15]. In brief, stock solutions of $(NH_4)_2HPO_4$ and $Ca(OH)_2$ were prepared by dissolving the precursors in distilled water. NaF was used as a source of F ions in this study. Pure and F ion substituted powder samples were prepared by dropwise addition of appropriate amounts of P and/or P+F ions containing precursor solutions into the stirring $Ca(OH)_2$ solution. Mixtures with different compositions were stirred for 10 min prior to transferring to a stainless autoclave reactor. After 8 h of hydrothermal treatment at 15.2 atm and 200 °C, the reacted powders were washed with distilled water and finally dried at 80 °C for 24 h. The fluoride ion content was determined by conducting F-selective electrode experiments. The composition of the samples selected for further characterization were $Ca_{10}(PO_4)_6(OH)_2$, $Ca_{10}(PO_4)_6(OH)_{1.33}F_{0.67}$, and $Ca_{10}(PO_4)_6(OH)_{0.58}F_{1.42}$, coded as HAp, FHAp-0.67, and FHAp-1.42 respectively.

2.2. Zeta potential measurement and particle size distribution

The effect of fluoride ion content on particle surface potential was determined by measuring the zeta potential. The powders were soaked in tris(hydroxymethyl)aminomethane (TRIS, Merck, Germany) solution buffered at pH 7 for 14 days prior to zeta potential measurement using Zetasizer (ZEN 3600) from Malvern instruments. The same procedure was performed for particle size determination using dynamic light scattering (DLS).

2.3. UV–visible spectroscopy

Preparation of the powder extracts were performed according to ISO 10993-12 procedure in which 1 ml of culture medium (RPMI) was added to 0.1 g of powder samples and incubated in a shaking incubator for 21 days at 37 °C with mild shaking. The powder samples were left for 6 h to settle down prior to test and the test samples were removed. Pure culture medium kept under the same condition was used as a control sample. Variation in medium chemistry was assessed by performing UV–visible spectroscopy (Shimadzu, 1601) in the 200–800 nm wavelength range at different time intervals including 1, 7, 14 and 21 days [16].

2.4. Protein adsorption assay

To determine protein adsorption, equal amount (1 mg/ml) of each powder composition in de-ionized water was mixed with diluted FBS (100 μg/ml). The particles settled after 24 h and the supernatant solutions were removed. The particles were rinsed once and twice with water prior to proteins adsorption test. In order to quantify the adsorbed proteins, the particles were washed with 0.01, 0.1, and 1 M potassium chloride solutions. Washing stage was repeated few times in order to detach all the adsorbed proteins. Subsequently, the amount of adsorbed proteins were analyzed by using protein determination assay based on the Bradford method [17]. The washing mediums were also resolved by performing SDS-polyacrylamide gel electrophoresis (SDS-PAGE) following the Bio-Rad instruction manual (Mini protein tetracell). Silver nitrate was used as a staining agent.

2.5. Determination of the specific surface area

The powders were dispersed in acetone using ultrasonic bath for 2 min and dropped on a pre-warmed glass slide. Atomic force microscopy (AFM, JPK, Germany) was operated in tapping mode using NSC15/AIBS tips on 5 randomly selected points. The specific surface area (SSA) was calculated from the sum of the specific edge surface area (ESA) and the specific basal surface area (BSA) according to the following equation based on the previous published procedures [18,19]. By using AFM images and JPK SPM data processing software, the height (h), the area (A), the perimeter (p) and the volume (V) of the powders were determined (ρ is the density of powder).

$$\mathrm{BSA} = 2 \times A/(\rho \times V) \quad (1)$$

$$\mathrm{ESA} = h \times p/(\rho \times V) \quad (2)$$

2.6. Viability test

In order to find the best concentration of the powder for gene expression assay, three different concentrations of the samples (10 mg/ml, 1 mg/ml and 0.1 mg/ml) were prepared in RPMI medium and kept at 37 °C for 21 days. The toxicity test was performed by the direct contact method after the cells exposed to each concentration directly without any settling or centrifugation. The human primary osteogenic sarcoma cell line MG63 (NCBI C-116; National Cell Bank of Iran, Pasteur Institute of Iran, Tehran, Iran) was cultured in RPMI medium supplemented with 10% fetal bovine serum, and antibiotics (100 U/ml penicillin and 100 μg/ml, streptomycin, Sigma, USA). The cells were

harvested using 0.25% trypsin–EDTA solution in phosphate-buffered saline (PBS; pH 7.4) and later were seeded on a 96 well culture plate at a density of 10×10^4 cells/well. The cultures were incubated at 37 °C in a humidified 5% CO_2 atmosphere for 24 h. Subsequently, the culture mediums were removed and powder extracts with 10% FBS were added to each well. After 24 hours, the extracts were removed and 100 μl neutral red solution in RPMI (40 μg/ml) was added to each well. The test plate was incubated for 3 h to incorporate the vital dye into survival cells. Then the medium was removed and rinsed rapidly in $CaCl_2$ (1%)/formaldehyde (1%) solution. Finally, the dye was extracted into 200 μl solution of acetic acid (1%)/ethanol (50%) for 10 min and the optical density of the samples was measured by a microplate reader (STAT FAX 2100, USA) at 540 nm.

2.7. RNA extraction and cDNA synthesis

Gene expression was analyzed by seeding 200 cells per each well in a 6 well culture plate the same as the toxicity procedure. After 24 h, the medium was removed and 0.1 mg of each sample in 1 ml culture medium (RPMI supplemented 10% FBS) added to the wells. The plate was incubated for 14 days at 37 °C with the addition of medium at the day 7. The extraction of total RNA from cultured cells was done at the day 14 using RNeasy MiniKit (QIAGEN, 74104) following the manufacturer's instructions. The concentration of cellular RNA was quantified by determining the maximum absorbance at 260 nm wavelength in a UV–visible spectrophotometer (Eppendorf, Germany). CDNA was obtained by mixing 1 μg of total RNA and 20 μl of reaction mixture including 4 μl PCR buffer (15X), 2 μl dNTPs (20 mM, Roche, Germany), 1 μl 10 pmol/μl random hexamer (N6; Roche, Germany), 2 μl deionized sterile H_2O and 1 μl reverse transcriptase (200 U/μl; Fermentase, Russia). Finally the mixture was kept at 42 °C for 45 min and then incubated at 90 °C for 5 min.

2.8. RT-PCR analysis

PCR amplification was performed using specific primers as collagen I FW: 5′ GGACACAATGGATTGCAAGG 3′, RV: 5′TAACCACTGCTCCACTCTGG 3′, alkaline phosphatase FW: 5′ TGGAGCTTGTCTGAGTACCAG TCC 3′, RV: 5′ ATCTCGTTGTCTGAGTACCAGTCC 3′ and GAPDH FW: 5′ GGGCTGCTTTTAACTCTGGT 3′, RV: 5′ TGGCAGGTTTTTCTAGACGG 3′ with the marker of GeneRuler™ 50 bp DNA ladder. For the next step, the mixture of 2.5 μl of 10X PCR buffer, 1 μl of 25 mM $MgCl_2$, 1.5 μl dNTPs (10 mM), 0.5 μl of each primer (10 pmol/ μl), 0.1 μl of Taq-DNA polymerase (5 U/μl; CinnaGen, Iran), and 3 μl of cDNA was prepared. Then 37 cycles of amplification were applied to the mixture consisting of 92 °C for 30 s, 62 °C for 30 s, 72 °C for 1 min and finally 72 °C for 10 min. After all agarose gel (2%) electrophoresis containing ethidium bromide was used for PCR products visualization.

2.9. Real time PCR analysis

The primer sequences specific for the target genes of collagen I (FW: 5′ GCCAAGACGAAGACATCCCA 3′, RV: 5′ CACACGTCTCGGTCATGG 3′), alkaline phosphatase (FW: 5′ TGGAGCTTCAGAAGCTCAACAC 3′, RV: 5′ TGGAGACACCCATCCCATCT 3′) and the internal

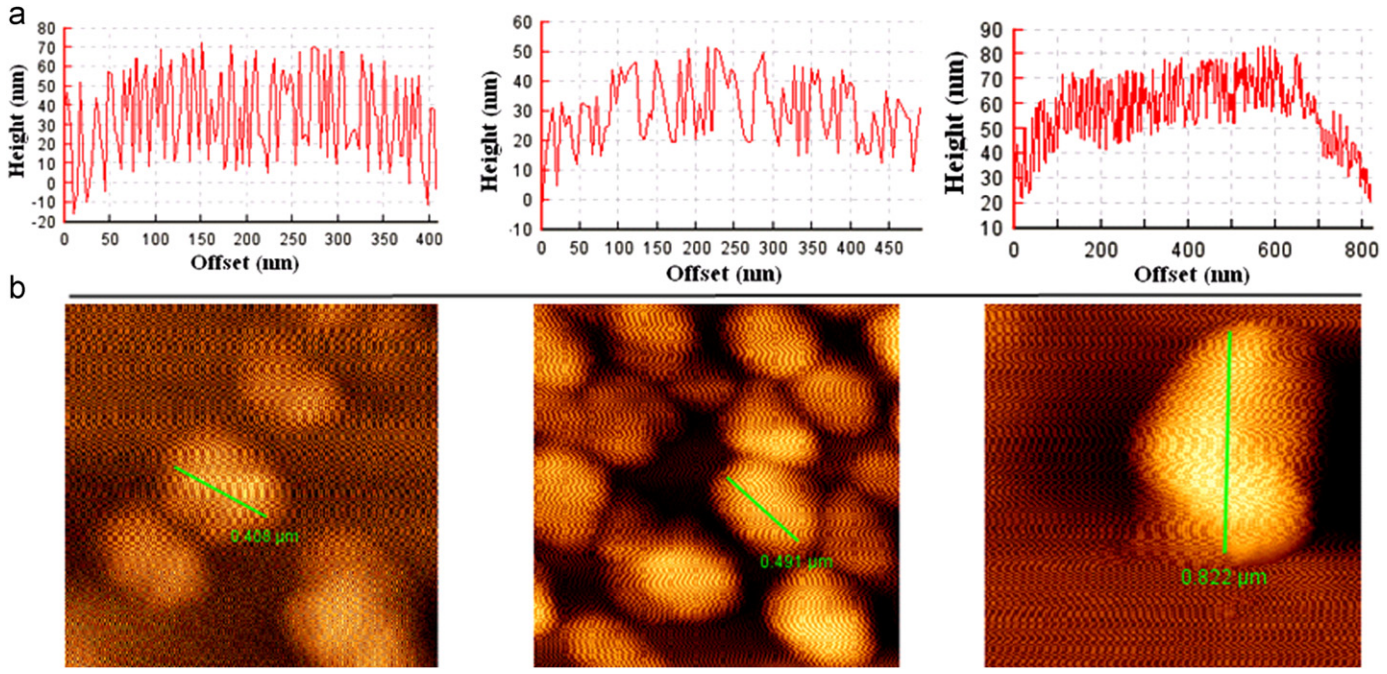

Fig. 1. AFM images of the samples with an approximation of their average size. (a)HAp, (b)FHAp-0.67 and (c)FHAp-1.42.

control gene GAPDH (FW: 5′ GAAGGTGAAGGTCG-GAGTC 3′, RV: 5′ GAAGATGGTGATGGGATTTC 3′) were used for qRT-PCR. The real-time PCR was performed in an ABI 7300 real-time PCR system (Applied Biosystems) with SYBR Green PCR master mix (Applied Biosystems).

3. Results and discussion

3.1. Zeta potential

The electrostatic interaction between the biomaterial surface and protein can be controlled by variation in the surface charge of adsorbents. In this study the effect of fluoride ion content on particle surface charge was determined by measuring the zeta potential. The findings showed 5.47, 6.56 and 6.61 mV potential for HAp, FHAp-0.67 and FHAp-1.42 respectively. The results obtained for hydroxyapatite are in agreement with the previous report [20]. Zeta potential determination is often performed to evaluate the electrostatic interaction between the particles surface and proteins. For instance, the favorable effect of positive zeta potential on albumin adsorption to the nano-ceria particles has already been observed in the literature [21]. There was an increase in the zeta potential values with the increase in

Table 1
Particle characterization by DLS and AFM, diameter and width were evaluated by DLS and specific surface area of each sample determined with AFM.

Simple	Particle diameter peak (nm)	Particle width peak (nm)	BSA $= 2 \times A/(\rho \times V)$ (m^2/g)	ESA $= h \times p/(\rho \times V)$ (m^2/g)	SSA (m^2/g)
HAp	409	34.71	25.00	5.83	30.83
FHAp-0.67	472	39.39	25.00	5.44	30.44
FHAp-1.42	831.6	140.8	14.29	3.66	17.94

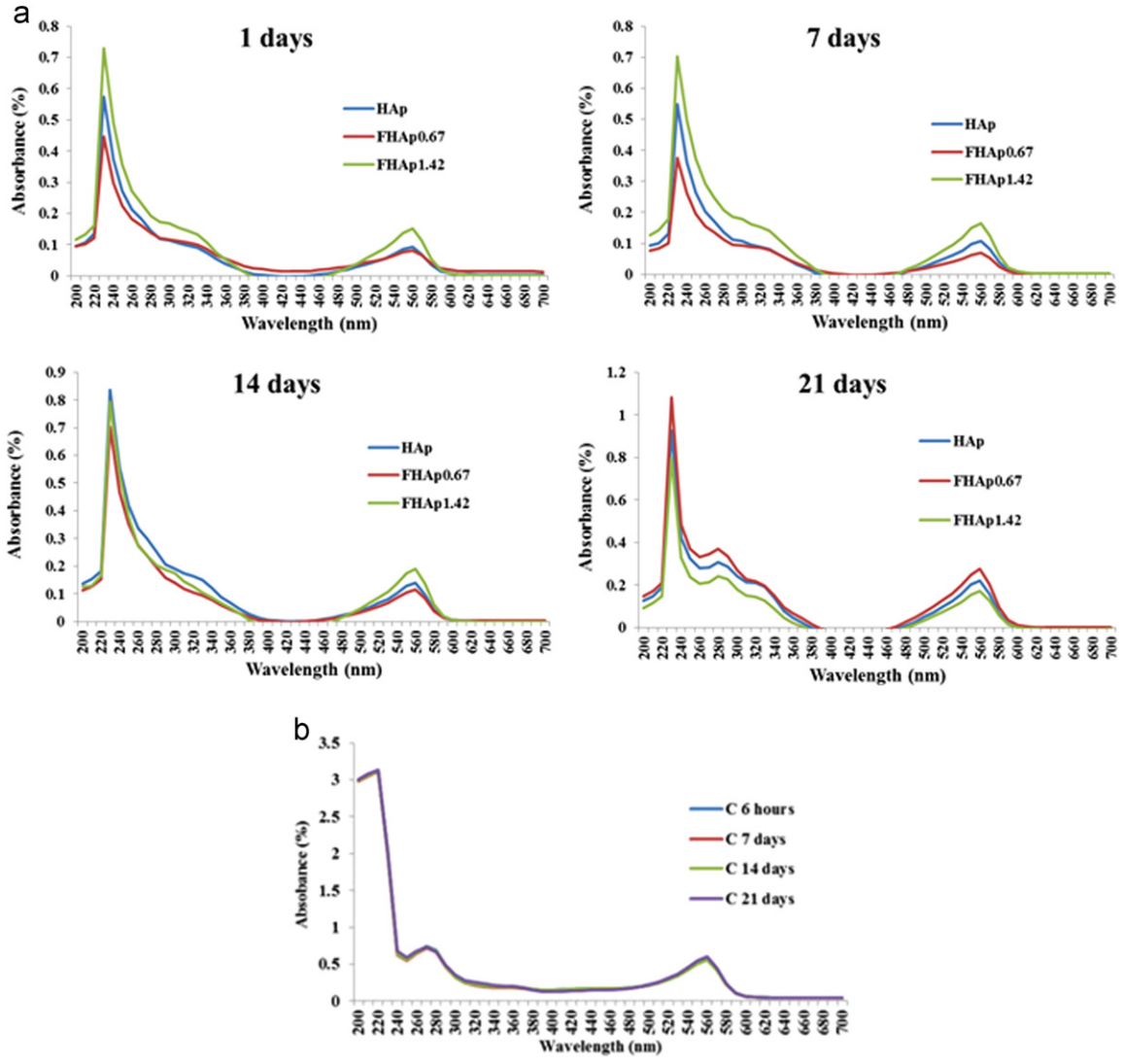

Fig. 2. (a) UV–visible spectra of powder extracts at different times and (b) UV–visible spectra of control samples.

fluoride ion substitution in the apatite structure. This behavior has been attributed to the attraction of more positive ions on particle surface due to the stronger electronegativity of fluoride ions [22].

3.2. AFM image

The specific surface area of each sample was determined by using extracted information from both AFM images and DLS (Fig. 1 and Table 1). FHAp-1.42 sample showed the lowest level of SSA, while the other two samples (HAp and FHAp-0.67) exhibited almost similar quantity. The thickness and length of the particles as well as agglomeration were raised by increase in fluoride substitution which is in agreement with Rameshbabu et al. report [23].

3.3. UV–visible spectroscopy

Variation of cell medium components due to the interaction with different powder compositions was analyzed using UV–visible spectroscopy. Fig. 2a presents UV/vis spectrum of powder in different time intervals (normalized to the control). Fig. 2b represents the UV spectra of the control samples. Incorporation of F ions in the apatite structure affects the amount of ionic release and the pH values in the medium. The medium color change associated with the change in pH values alters the absorption band intensity at 560 nm as indicated in Fig. 2. The absorption band at 240 nm is believed to be related to the variation of culture medium composition [16]. As demonstrated in the spectra, the same trend for all the samples can be observed. FHAp-0.67 and FHAp-1.42 respectively showed the least and the highest amount of medium component absorption until day 14 while it changed at day 21. The cell culture mediums contain different components and each one may be adsorbed by the test samples and desorb through the test process.

3.4. Protein adsorption

The amount of serum protein adsorbed on the samples with different compositions is illustrated in Fig. 3. As shown in this diagram, the powder sample coded as FHAp-0.67 absorbed more FBS proteins compared to the other samples. As pointed out earlier the extent of interaction of the biomaterial with the protein is determined largely by the surface characteristics of biomaterial. From the results shown in Fig. 3, it may be concluded that initially the increase in surface zeta potential values works in favor of more protein adsorption (sample FHAp-0.67). However, at higher substitution levels (sample FHAp-1.42) a reduction in protein adsorption was observed as indicated in Fig. 3. In other words, there is a reduction in protein binding affinity of the apatite structure with the increase in fluoride ion substitution in the structure. The results implicate the importance of hydroxyl groups as protein binding sites. The contact surface of the powder and protein is another important parameter in protein adsorption. In this study, it was found that at higher fluoride content the diameter of the particles increased and specific surface area decreased. Therefore, the amount of fluoride in apatite structure is critical for protein adsorption due to both the chemical and physical variations. In addition, types of protein, period of exposure and environmental conditions also dictate the amount of adsorption. It should also be mentioned that washing the particle surfaces with 0.1 M potassium chloride solution was more effective in isolating the adsorbed proteins.

3.5. SDS-PAGE analysis

Fig. 4 displays the results of the SDS-PAGE analysis. Columns 1–3 present the results on the FBS+water

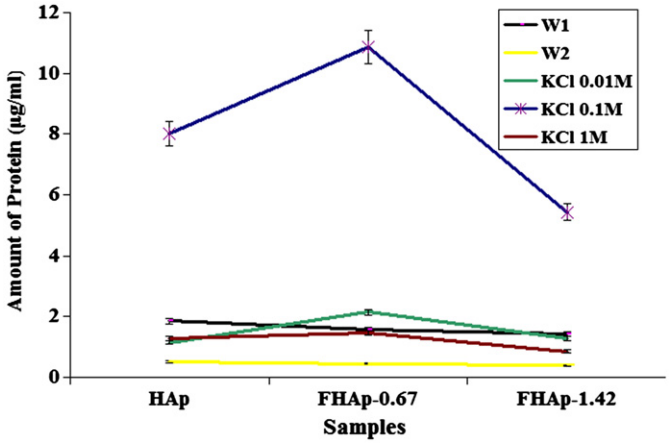

Fig. 3. The amount of protein adsorbed on different particle surfaces determined after washing once and twice with water (W1 and W2) and KCl (0.01, 0.1 and 1 M) solutions.

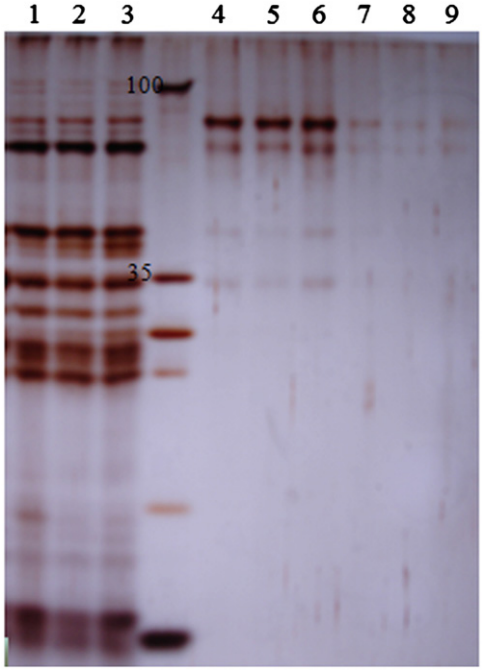

Fig. 4. SDS-PAGE analysis. Columns 1–3 present the results on the FBS+water solutions after 24 h exposure to HAp, FHAp-0.67 and FHAp-1.42 powder samples respectively. Columns 4–6 and 6–9 are the analysis on 0.1 and 0.01 M KCl washing mediums respectively.

solutions after 24 h exposure to HAp, FHAp-0.67 and FHAp-1.42 powder samples respectively. Columns 4–6 and 6–9 are the analysis on 0.1 and.01 M KCl washing mediums respectively. A closer examination of columns 1–3 shows the bands of unattached proteins to the surface of the samples. The appearance of a band at 80 KDa after washing the particles with 0.1 M KCl solution, suggests a preferential adsorption of proteins with molecular weight of 80 kDa on the surface of the powders (columns 4–6). These findings confirm the results of Bradford analysis too and show that the solution of 0.01 M KCl cannot detach the protein from particles while increase in KCl concentration to 0.1 M, can lose the protein attachment. This concentration (0.1 M KCl) is sufficient for protein separation and concentration of 1 M KCl, did not show any change in the amount of washed protein.

Due to the large surface area/volume ratio nanoparticles tend to agglomerate and adsorb proteins. The high affinity of hydroxyapatite to proteins has been reported previously [24]. For example, adsorption of lysozyme and salivary proteins to these particles has been confirmed [25,26]. It has been reported that the adsorption of enamel proteins is enhanced by increasing fluoride content in HA structure [27]. Also, increase in fluoride content of hydroxyapatite discs results in decrease of statherin and histatin and increase of basic proline rich protein 2 adsorption [28]. Eggen and Rolla showed that desorption of albumin from hydroxyapatite is enhanced by the presence of fluoride in the structure while others reported that the albumin adsorption depends on the fluoride concentration [29,30]. This dependence may enhance or inhibit serum protein adsorption on the material surfaces. Therefore, optimizing the fluoride content in the composition may significantly improve the biological response [22].

3.6. Viability assay

According to the ISO10993-12, cell toxicity evaluation needs at least 100 mg/ml concentration of the powders. Although this concentration did not show any chemical toxicity [15], the precipitation of these powders above the cell layer may physically cover the cell surface and cause cell death. The osteoblast cells were exposed directly to the samples with different concentrations (0.1, 1 and 10 mg/ml) in order to find the non-lethal dilution ratio. Fig. 5 shows the results of cell viability after neutral red staining and confirms the viability of the cells exposed to 0.1 mg/ml concentration compared to control.

3.7. RT-PCR results

Both qualitative and quantitative PCR results are presented in Fig. 6. As seen in this figure, the low fluoride containing sample (FHAp-0.67) showed the highest collagen I and ALP activity levels. The positive influence of F

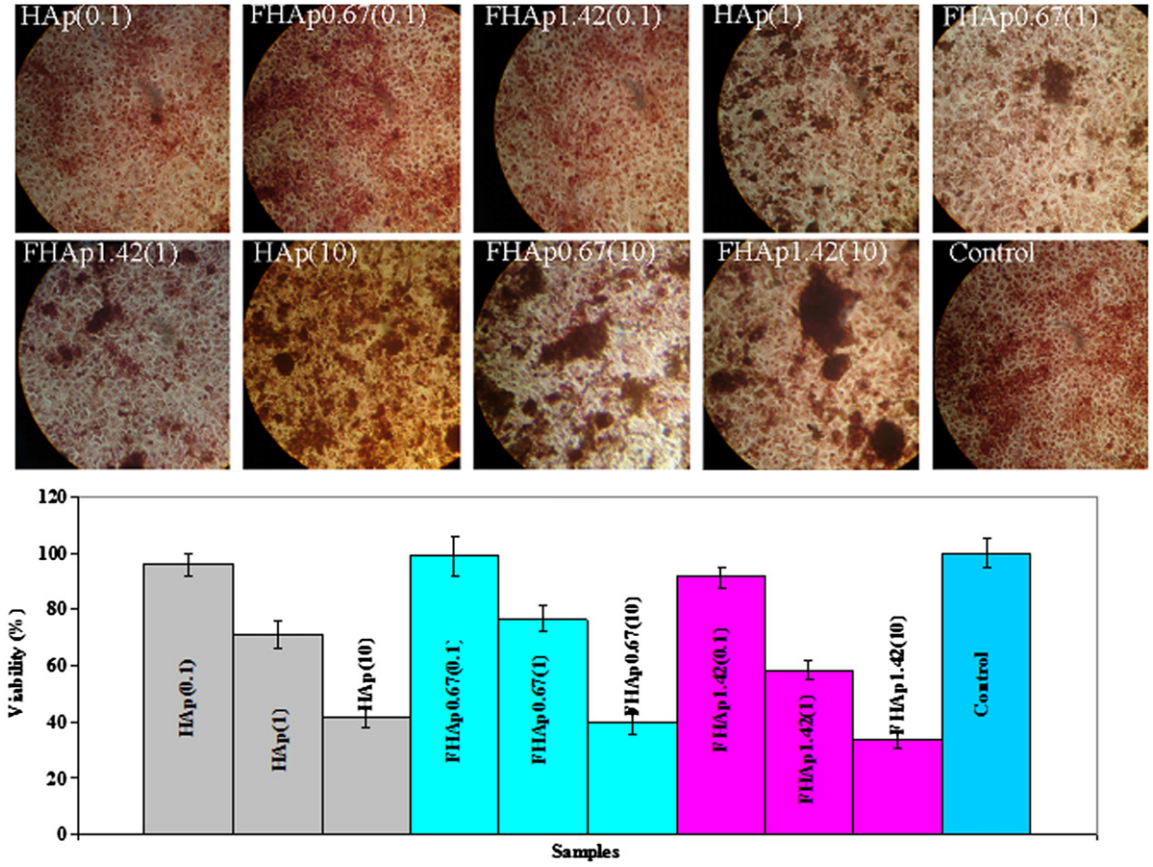

Fig. 5. The osteoblast cell proliferation exposed to the samples. 0.1 mg/ml concentration shows the cells viability compare with control (magnification × 200).

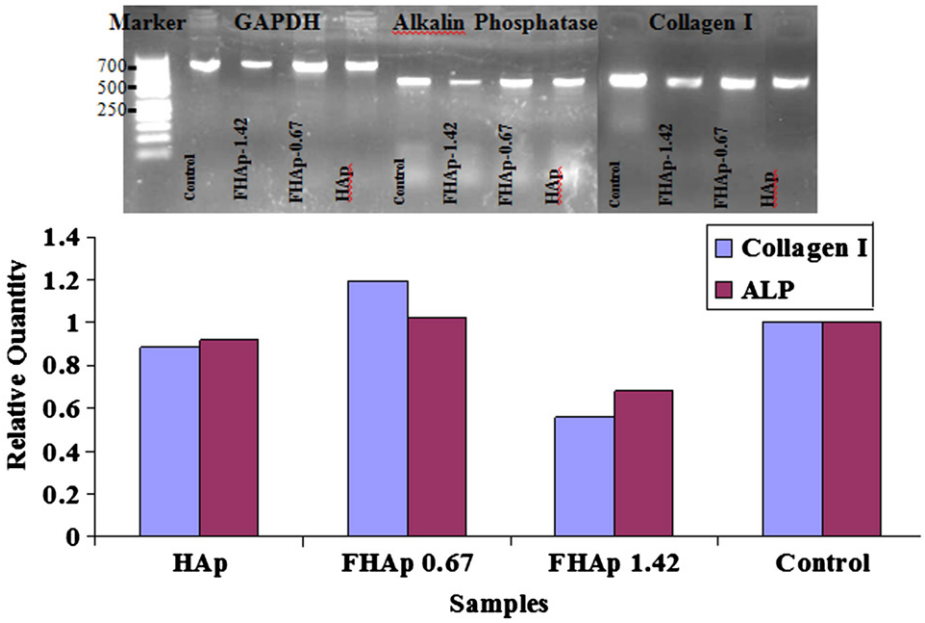

Fig. 6. PCR results (quantitative and qualitative) for collagen I and ALP activity. The results were normalized with glyceraldehyde-3-phosphate dehydrogenase (GAPDH).

ions on osteoblastic cell attachment, proliferation, differentiation as well as extracellular matrix (ECM) protein secretion has already been reported in the literature [31–33]. Furthermore, as indicated in Fig. 6 the powder sample containing more F ions (FHAp-1.42) showed the least collagen I and ALP expression levels. The results presented in Figs. 3–5 are consistent with earlier reports, that only a moderate content of F ions in the apatite structure is most suitable in improving the cellular productions [30–33].

4. Conclusions

The effect of fluoride ion concentration in the apatite structure on protein adsorption was investigated. It was found that an increase in the fluoride ion content changes the biological performance of the powder in a dose and time dependent manner and more protein was adsorbed on a powder with moderate amount of fluoride substitution in the structure. This sample also exhibited higher level of collagen I and alkaline phosphatase expression levels. Additional in vivo experiments are in progress to investigate the effect of ionic substitution on the apatite powder behavior when exposed to the circulating blood protein at various times.

Acknowledgment

Authors would like to express their appreciation to the Iranian Pasteur Institute for its financial assistance.

References

[1] Y. Yong, S.S. Kulkarni, M. Rys, S. Lei, Development of a surface roughness model in end milling of nHAP using PCD insert, Ceramics International 38 (8) (2012) 6865–6871.
[2] K.A. Gross, K.A. Bhadang, Sintered hydroxyfluorapatites. Part III: sintering and resultant mechanical properties of sintered blends of hydroxyapatite and fluorapatite,, Biomaterials 25 (7–8) (2004) 1395–1405.
[3] K.A. Bhadang, K.A. Gross, Influence of fluorapatite on the properties of thermally sprayed hydroxyapatite coatings, Biomaterials 25 (20) (2004) 4935–4945.
[4] M. Kheradmandfard, M.H. Fathi, M. Ahangarian, E.M. Zahrani, In vitro bioactivity evaluation of magnesium-substituted fluorapatite nanopowders, Ceramics International 38 (1) (2012) 169–175.
[5] N. Johari, M.H. Fathi, M.A. Golozar, The effect of fluorine content on the mechanical properties of poly (ε-caprolactone)/nano-fluoridated hydroxyapatite scaffold for bone-tissue engineering, Ceramics International 37 (8) (2011) 3247–3251.
[6] A. Aminian, M. Solati-Hashjin, A. Samadikuchaksaraei, F. Bakhshi, F. Gorjipour, A. Farzadi, F. Moztarzadeh, M. Schmücker, Synthesis of silicon-substituted hydroxyapatite by a hydrothermal method with two different phosphorous sources, Ceramics International 37 (4) (2011) 1219–1229.
[7] A. Bianco, I. Cacciotti, M. Lombardi, L. Montanaro, E. Bemporad, M. Sebastiani, F-substituted hydroxyapatite nanopowders: thermal stability, sintering behaviour and mechanical properties, Ceramics International 36 (1) (2010) 313–322.
[8] S. Zhang, Y.S. Wang, X.T. Zeng, K.A. Khor, W.J. Weng, D.E. Sun, Evaluation of adhesion strength and toughness of fluoridated hydroxyapatite coatings, Thin Solid Films 516 (16) (2008) 5162–5167.
[9] K.A. Gross, L.M. Rodriguez-Lorenzo, Sintered hydroxyfluorapatites. Part II: mechanical properties of solid solutions determined by microindentation,, Biomaterials 25 (7–8) (2004) 1385–1394.
[10] B. Basar, A. Tezcaner, D. Keskin, Z. Evis, Improvements in microstructural, mechanical, and biocompatibility properties of nano-sized hydroxyapatites doped with yttrium and fluoride, Ceramics International 36 (5) (2010) 1633–1643.

[11] K. Cheng, S. Zhang, W.J. Weng, X.T. Zeng, The interfacial study of sol–gel-derived fluoridated hydroxyapatite coatings, Surface and Coatings Technology 198 (1–3) (2005) 242–246.
[12] A.E. Nel, L. Madler, D. Velegol, T. Xia, E.M.V. Hoek, P. Somasundaran, F. Klaessig, V. Castranova, M. Thompson, Understanding biophysicochemical interactions at the nano-bio interface, Nature Materials 8 (7) (2009) 543–557.
[13] K.M. Hennessy, B.E. Pollot, W.C. Clem, M.C. Phipps, A.A. Sawyer, B.K. Culpepper, S.L. Bellis, The effect of collagen I mimetic peptides on mesenchymal stem cell adhesion and differentiation, and on bone formation at hydroxyapatite surfaces, Biomaterials 30 (10) (2009) 1898–1909.
[14] A.A. Sawyer, K.M. Hennessy, S.L. Bellis, Regulation of mesenchymal stem cell attachment and spreading on hydroxyapatite by RGD peptides and adsorbed serum proteins, Biomaterials 26 (13) (2005) 1467–1475.
[15] L. Montazeri, J. Javadpour, M.A. Shokrgozar, S. Bonakdar, S. Javadian, Hydrothermal synthesis and characterization of hydroxyapatite and fluorhydroxyapatite nano-size powders, Biomedical Materials 5 (4) 045004.
[16] M. Mahmoudi, A. Simchi, M. Imani, A.S. Milani, P. Stroeve, An in vitro study of bare and poly(ethylene glycol)-co-fumarate-coated superparamagnetic iron oxide nanoparticles: a new toxicity identification procedure, Nanotechnology 20 (22) (2009) 225104.
[17] B.J.S.C. Olson, J. Markwell, Assays for determination of protein concentration, Current Protocols in Protein Science, John Wiley and Sons, Inc., 2001.
[18] B.R. Bickmore, K.L. Nagy, P.E. Sandlin, T.S. Crater, Quantifying surface areas of clays by atomic force microscopy, American Mineralogist 87 (5–6) (2002) 780–783.
[19] F. Macht, K. Eusterhues, G.J. Pronk, K.U. Totsche, Specific surface area of clay minerals: comparison between atomic force microscopy measurements and bulk-gas (N_2) and -liquid (EGME) adsorption methods, Applied Clay Science 53 (1) 20–26.
[20] E. Landi, G. Logroscino, L. Proietti, A. Tampieri, M. Sandri, S. Sprio, Biomimetic Mg-substituted hydroxyapatite: from synthesis to in vivo behaviour,, Journal of Materials Science: Materials in medicine 19 (1) (2008) 239–247.
[21] S. Patil, A. Sandberg, E. Heckert, W. Self, S. Seal, Protein adsorption and cellular uptake of cerium oxide nanoparticles as a function of zeta potential, Biomaterials 28 (31) (2007) 4600–4607.
[22] K. Cheng, W. Weng, H. Wang, S. Zhang, In vitro behavior of osteoblast-like cells on fluoridated hydroxyapatite coatings, Biomaterials 26 (32) (2005) 6288–6295.
[23] N. Rameshbabu, T.S.S. Kumar, K.P. Rao, Synthesis of nanocrystalline fluorinated hydroxyapatite by microwave processing and its in vitro dissolution study, Bulletin of Materials Science 29 (6) (2006) 611–615.
[24] K. Kandori, K. Murata, T. Ishikawa, Microcalorimetric study of protein adsorption onto calcium hydroxyapatites, Langmuir: The ACS Journal of Surfaces and Colloids 23 (4) (2007) 2064–2070.
[25] K. Kandori, N. Horigami, H. Kobayashi, A. Yasukawa, T. Ishikawa, Adsorption of lysozyme onto various synthetic hydroxyapatites, Journal of Colloid and Interface Science 191 (2) (1997) 498–502.
[26] M.S. Lamkin, A.A. Arancillo, F.G. Oppenheim, Temporal and compositional characteristics of salivary protein adsorption to hydroxyapatite, Journal of Dental Research 75 (2) (1996) 803–808.
[27] T. Tanabe, T. Aoba, E.C. Moreno, M. Fukae, Effect of fluoride in the apatitic lattice on adsorption of enamel proteins onto calcium apatites, Journal of Dental Research 67 (3) (1988) 536–542.
[28] W.L. Siqueira, M. Bakkal, Y. Xiao, J.N. Sutton, F.M. Mendes, Quantitative proteomic analysis of the effect of fluoride on the acquired enamel pellicle, PloS One 7 (8) e42204.
[29] K.H. Eggen, G. Rolla, The effect of fluoride on the uptake of albumin by hydroxyapatite, Caries Research 16 (4) (1982) 282–286.
[30] D.T. Wassell, R.C. Hall, G. Embery, Adsorption of bovine serum albumin onto hydroxyapatite, Biomaterials 16 (9) (1995) 697–702.
[31] J.R. Farley, J.E. Wergedal, D.J. Baylink, Fluoride directly stimulates proliferation and alkaline phosphatase activity of bone-forming cells, Science 222 (4621) (1983) 330–332.
[32] H. Qu, M. Wei, The effect of fluoride contents in fluoridated hydroxyapatite on osteoblast behavior, Acta biomaterialia 2 (1) (2006) 113–119.
[33] J.M. Gibson, J.M. Popham, V. Raghunathan, P.S. Stayton, G.P. Drobny, A solid-state NMR study of the dynamics and interactions of phenylalanine rings in a statherin fragment bound to hydroxyapatite crystals, Journal of the American Chemical Society 128 (16) (2006) 5364–5370.